Optimized mechanical quadrature squeezing beyond the 3-dB limit via a gradient-descent algorithm

Yu-Hong Liu [1] and Jie-Qiao Liao [1,2,*]

[1] *Key Laboratory of Low-Dimensional Quantum Structures and Quantum Control of Ministry of Education, Key Laboratory for Matter Microstructure and Function of Hunan Province, Department of Physics and Synergetic Innovation Center for Quantum Effects and Applications, Hunan Normal University, Changsha 410081, China*

[2] *Institute of Interdisciplinary Studies, Hunan Normal University, Changsha 410081, China*

(Received 19 May 2024; accepted 7 August 2024; published 22 August 2024)

The preparation of mechanical quadrature-squeezed states holds significant importance in cavity optomechanics because the squeezed states have extensive applications in understanding fundamental quantum mechanics and exploiting modern quantum technology. Here, we propose a reliable scheme for generating mechanical quadrature squeezing in a typical cavity optomechanical system via seeking optimal cavity-field driving pulses using the gradient-descent algorithm. We realize strong quadrature squeezing in a mechanical resonator that exceeds the 3-dB steady-state limit, even with a thermal phonon occupancy of 100. Furthermore, the mechanical squeezing can be ultrarapidly created within one mechanical oscillation period. We also obtain the optimal pulsed drivings associated with the created mechanical squeezings and analyze the mechanism for mechanical squeezing generation. This paper will promote the application of optimal quantum control in quantum optics and quantum information science.

DOI: 10.1103/PhysRevA.110.023519

I. INTRODUCTION

Cavity optomechanics [1] is a frontier research field focusing on the radiation-pressure interaction between cavity fields and moving mirrors at macroscopic scales. Owing to the nonlinear properties of the optomechanical interaction and the development of laser cooling techniques [2–5], optomechanical systems provide new paths and opportunities for generation and manipulation of macroscopic nonclassical states, such as entangled states [6–11], quantum superposed states [12–15], and squeezed states of fields [16–21] and mechanical resonators [22–44].

Quantum squeezing, as an essential quantum resource, plays an increasingly significant role in modern quantum technology ranging from quantum precision measurement to quantum information processing [45,46]. Quantum squeezing of mechanical modes holds significance as it has the potential to enhance the accuracy of quantum measurements [47]. There exist many theoretical and experimental schemes for generating mechanical squeezing based on various methods, such as parametric squeezing [25–32], quantum measurement [33–37], quantum state transfer [38–40], mechanical nonlinearities [25,41,42], and reservoir engineering [43,44]. In particular, some methods [26,29,30,34,38,41–43] can be used to generate the quadrature squeezing, which exceeds the 3-dB squeezing limit [27,48]. The strong squeezing has wide applications in quantum technology, and its generation is a significant task in quantum optics. In addition, from the viewpoint of realistic application, an ultrafast generation of strong mechanical squeezing remains a challenge.

In cavity optomechanical systems, the external optical driving provides an effective way to control the quantum properties and dynamical behaviors of the system [26,28,49–51]. The design of an optimal optical driving to achieve a supposed goal is an interesting topic in this system. Currently, quantum control techniques have been successfully applied to various schemes in cavity optomechanical systems [52], such as robust state transfer [53], optimized cooling [54–56], entanglement enhancement [57,58], and strong squeezing [59,60]. Furthermore, optimal control technology based on the gradient-descent algorithm [61] has been recognized as a powerful method to accomplish complex control tasks, and hence it is expected to provide new ways to optimize the control of cavity optomechanical systems.

In this paper, we apply the gradient-descent algorithm to prepare mechanical quadrature squeezing in a typical cavity optomechanical system. Our scheme can break the 3-dB steady-state squeezing limit even when the environment thermal phonon occupation associated with the mechanical resonator reaches the order of 100. The mechanical quadrature squeezing is achieved by designing a proper pulsed driving to the cavity field. Concretely, we use the gradient-descent algorithm to iteratively optimize the pulsed driving for achieving strong mechanical squeezing. The optimal waveforms of the pulsed driving amplitude and phase are also obtained. In particular, mechanical squeezing can be ultrarapidly prepared within one mechanical oscillation period, providing more chance for realistic applications of the generated squeezing before decoherence. Our method will encourage further researches on optimal quantum control in cavity optomechanical systems.

*Contact author: jqliao@hunnu.edu.cn

The rest of this paper is organized as follows. In Sec. II, we introduce the Hamiltonians and present the equations of motion. In Sec. III, we show the generation of mechanical quadrature squeezing using the gradient-descent algorithm. In Sec. IV, we present some discussions concerning the influences of driving amplitude and phase noises on the squeezing generation, the physical mechanism of the present squeezing-generation method, the experimental implementation of this squeezing-generation scheme, and the applications of the optimization methods in cavity optomechanics. Finally, we conclude this paper in Sec. V. The Appendix shows the derivation of the variation $\delta[\Delta X_b^2(\theta,T)]/\delta\mathcal{Q}_m$ used in the gradient-descent algorithm.

II. HAMILTONIANS AND EQUATIONS OF MOTION

We consider a typical cavity optomechanical system that consists of a mechanical resonator optomechanically coupled to a single-mode cavity field. To control the dynamics of the system, the cavity mode is driven by a strong pulsed field with carrier frequency $\omega_{\rm L}$, driving amplitude $\Omega(t)$, and driving phase $\phi(t)$. In a rotating frame defined by the unitary operator $\exp(-i\omega_{\rm L}ta^\dagger a)$, the Hamiltonian of the system reads ($\hbar=1$)

$$H_{\rm opt}(t)=\Delta_{\rm c}a^\dagger a+\omega_{\rm m}b^\dagger b-g_0a^\dagger a(b^\dagger+b)+[\Omega(t)e^{-i\phi(t)}a^\dagger+{\rm H.c.}],\tag{1}$$

where $a^\dagger$ (a) and $b^\dagger$ (b) are, respectively, the creation (annihilation) operators of the cavity field and the mechanical resonator, with the corresponding resonance frequencies $\omega_{\rm c}$ and $\omega_{\rm m}$. The $\Delta_{\rm c}=\omega_{\rm c}-\omega_{\rm L}$ is the detuning of the cavity-field resonance frequency with respect to the pulsed-field carrier frequency. The g_0 term describes the radiation-pressure coupling between the cavity field and the mechanical resonator, with g_0 being the single-photon optomechanical-coupling strength.

In the open-system case, we assume that the cavity field is coupled to a vacuum bath, while the mechanical resonator is connected to a heat bath. Considering the Markovian dissipations, the evolution of the system is governed by the quantum master equation

$$\dot\rho=i[\rho,H_{\rm opt}(t)]+\kappa\mathcal{D}[a]\rho+\gamma(\bar n_{\rm m}+1)\mathcal{D}[b]\rho+\gamma\bar n_{\rm m}\mathcal{D}[b^\dagger]\rho,\tag{2}$$

where ρ is the density matrix of the optomechanical system, $\mathcal{D}[o]\rho=o\rho o^\dagger-(o^\dagger o\rho+\rho o^\dagger o)/2$ (for $o=a$, $a^\dagger$, b, and $b^\dagger$) is the Lindblad superoperator [62], and $H_{\rm opt}(t)$ is defined in Eq. (1). The parameters κ and γ are, respectively, the damping rates of the cavity field and the mechanical resonator, and $\bar n_{\rm m}$ is the environmental thermal-excitation occupation of the mechanical resonator.

Considering the strong-driving case of the optomechanical cavity, then the dynamics of the system can be linearized. To this end, we adopt the displacement-transformation method to separate the semiclassical motion and quantum fluctuation. Concretely, we perform the displacement transformations $D_a(\alpha)=\exp(\alpha a^\dagger-\alpha^* a)$ and $D_b(\beta)=\exp(\beta b^\dagger-\beta^* b)$ for the density operator $\rho(t)$, namely,

$$\rho'(t)=D_a(\alpha)D_b(\beta)\rho(t)D_b^\dagger(\beta)D_a^\dagger(\alpha),\tag{3}$$

where $\rho'(t)$ represents the density operator in the displaced representation, and $\alpha(t)$ and $\beta(t)$ are the displacement amplitudes of the cavity field and the mechanical resonator, respectively. By substituting $\rho(t)=D_b^\dagger(\beta)D_a^\dagger(\alpha)\rho'(t)D_a(\alpha)D_b(\beta)$ into Eq. (2) and setting the coefficients of the driving terms to be zero, we obtain the quantum master equation in the displaced representation as

$$\dot\rho'=i[\rho',H_{\rm dis}(t)]+\kappa\mathcal{D}[a]\rho'+\gamma(\bar n_{\rm m}+1)\mathcal{D}[b]\rho'+\gamma\bar n_{\rm m}\mathcal{D}[b^\dagger]\rho',\tag{4}$$

where $H_{\rm dis}(t)$ is the Hamiltonian in the displaced representation, defined as

$$H_{\rm dis}(t)=\Delta(t)a^\dagger a+\omega_{\rm m}b^\dagger b-g_0a^\dagger a(b+b^\dagger)+[G(t)a^\dagger+G^*(t)a](b+b^\dagger).\tag{5}$$

In Eq. (5), we introduce the linearized optomechanical-coupling strength $G(t)=g_0\alpha(t)$ and the normalized driving detuning $\Delta(t)=\Delta_c+g_0[\beta(t)+\beta^*(t)]$. The two displacement amplitudes $\alpha(t)$ and $\beta(t)$ are governed by the equations of motion

$$\dot\alpha(t)=-\left[i\Delta(t)+\frac{\kappa}{2}\right]\alpha(t)+i\Omega(t)e^{-i\phi(t)},\tag{6a}$$

$$\dot\beta(t)=-\left(i\omega_{\rm m}+\frac{\gamma}{2}\right)\beta(t)-ig_0|\alpha(t)|^2.\tag{6b}$$

In the strong-driving case, $|\alpha(t)|\gg1$, we can safely omit the g_0 term in Eq. (5), and obtain the linearized optomechanical Hamiltonian

$$H_{\rm lin}(t)=\Delta(t)a^\dagger a+\omega_{\rm m}b^\dagger b+[G(t)a^\dagger+G^*(t)a](b+b^\dagger).\tag{7}$$

Since both the linearized optomechanical-coupling strength $G(t)$ and the normalized driving detuning $\Delta(t)$ in Hamiltonian (7) depend on $\alpha(t)$ and $\beta(t)$, the dynamic evolution of the system can be controlled by adjusting the amplitude and phase of the pulsed driving, as shown by Eqs. (6a) and (6b). The dynamic properties of the linearized optomechanical system are completely described by both the first- and second-order moments of the system operators. Using the relation $\partial_t\langle o_io_j\rangle={\rm Tr}(\dot\rho' o_io_j)$ for $o_i,o_j\in\{a,a^\dagger,b,b^\dagger\}$ and Eq. (4) under the replacement of $H_{\rm dis}(t)\to H_{\rm lin}(t)$, we obtain the equations of motion of all these second-order moments, which can be expressed as

$$\dot{\mathbf{X}}(t)=\mathbf{M}(t)\mathbf{X}(t)+\mathbf{N}(t),\tag{8}$$

where $\mathbf{X}(t)=(\langle a^\dagger a\rangle,\langle b^\dagger b\rangle,\langle a^\dagger b\rangle,\langle ab^\dagger\rangle,\langle a^\dagger a^\dagger\rangle,\langle a^\dagger b^\dagger\rangle,\langle b^\dagger b^\dagger\rangle,\langle aa\rangle,\langle ab\rangle,\langle bb\rangle)^{\rm T}$ ("T" denotes the matrix transpose), $\mathbf{N}(t)=(0,\gamma\bar n_{\rm m},0,0,0,ig_0\alpha^*,0,0,-ig_0\alpha,0)^{\rm T}$, and the

coefficient matrix is introduced as $\mathbf{M}(t)=\begin{pmatrix}\mathbf{H} & \mathbf{I}\\ \mathbf{J} & \mathbf{K}\end{pmatrix}$, with

$$\mathbf{H}=\begin{pmatrix}-\kappa & 0 & -ig_0\alpha & ig_0\alpha^*\\ 0 & -\gamma & ig_0\alpha & -ig_0\alpha^*\\ -ig_0\alpha^* & ig_0\alpha^* & K_1 & 0\\ ig_0\alpha & -ig_0\alpha & 0 & K_1^*\end{pmatrix}, \tag{9a}$$

$$\mathbf{I}=\begin{pmatrix}0 & -ig_0\alpha & 0 & 0 & ig_0\alpha^* & 0\\ 0 & -ig_0\alpha & 0 & 0 & ig_0\alpha^* & 0\\ -ig_0\alpha & 0 & 0 & 0 & 0 & ig_0\alpha^*\\ 0 & 0 & -ig_0\alpha & ig_0\alpha^* & 0 & 0\end{pmatrix}, \tag{9b}$$

$$\mathbf{J}=\begin{pmatrix}0 & 0 & 2ig_0\alpha^* & 0\\ ig_0\alpha^* & ig_0\alpha^* & 0 & 0\\ 0 & 0 & 0 & 2ig_0\alpha^*\\ 0 & 0 & 0 & -2ig_0\alpha\\ -ig_0\alpha & -ig_0\alpha & 0 & 0\\ 0 & 0 & -2ig_0\alpha & 0\end{pmatrix}, \tag{9c}$$

$$\mathbf{K}=\begin{pmatrix}K_2 & 2ig_0\alpha^* & 0 & 0 & 0 & 0\\ ig_0\alpha & K_3 & ig_0\alpha^* & 0 & 0 & 0\\ 0 & 2ig_0\alpha & K_4 & 0 & 0 & 0\\ 0 & 0 & 0 & K_2^* & -2ig_0\alpha & 0\\ 0 & 0 & 0 & -ig_0\alpha^* & K_3^* & 0\\ 0 & 0 & 0 & 0 & -2ig_0\alpha^* & K_4^*\end{pmatrix}. \tag{9d}$$

In Eq. (9), we introduce

$$K_1=i\Delta(t)-i\omega_{\rm m}-\tfrac{1}{2}(\kappa+\gamma), \tag{10a}$$

$$K_2=2i\Delta(t)-\kappa, \tag{10b}$$

$$K_3=i\Delta(t)+i\omega_{\rm m}-\tfrac{1}{2}(\kappa+\gamma), \tag{10c}$$

$$K_4=2i\omega_{\rm m}-\gamma. \tag{10d}$$

We point out that both the coefficient matrix $\mathbf{M}(t)$ and the inhomogeneous term $\mathbf{N}(t)$ are functions of the displacement amplitudes $\alpha(t)$ and $\beta(t)$, thus the dynamic evolution of the second-order moments can be controlled via adjusting the pulsed driving.

III. GENERATION OF MECHANICAL QUADRATURE SQUEEZING

To quantify the created mechanical squeezing, we introduce the quadrature operators $X_{o=a,b}=(o^\dagger+o)/\sqrt{2}$ and $Y_{o=a,b}=i(o^\dagger-o)/\sqrt{2}$ for the optical and mechanical modes. Then the transient correlation matrix can be introduced as

$$\mathbf{V}_{ij}(t)=\tfrac{1}{2}[\langle\mathbf{u}_i(t)\mathbf{u}_j(t)\rangle+\langle\mathbf{u}_j(t)\mathbf{u}_i(t)\rangle]+\langle\mathbf{u}_i(t)\rangle\langle\mathbf{u}_j(t)\rangle, \tag{11}$$

where $\mathbf{u}(t)=(X_a(t),Y_a(t),X_b(t),Y_b(t))^{\rm T}$. In the present case, the expectation values $\langle\mathbf{u}_i(t)\rangle$ and $\langle\mathbf{u}_j(t)\rangle$ are zero and $\langle\mathbf{u}_i(t)\mathbf{u}_j(t)\rangle$ is a linear function of these second-order moments. To describe the quadrature squeezing, we further introduce the rotating-quadrature operator

Algorithm 1. Mechanical squeezing generation.

Input: A randomly smooth and continuous initial pulsed driving with amplitude Ω and phase ϕ.
Define: The loss function $\Delta X_b^2(\theta,T)$.
While $\Delta X_b^2(\theta,T)>\epsilon$ (ϵ is the expected value) **do**:
1. Perform the gradient-descent algorithm $\mathcal{Q}_{m+1}=\mathcal{Q}_m-\chi_{\mathcal{Q}}\{\delta[\Delta X_b^2(\theta,T)]/\delta\mathcal{Q}_m\}$ ($\mathcal{Q}$ represents either Ω or ϕ, $\chi_{\mathcal{Q}}$ is the learning rate, and m indicates the iteration number) to iteratively minimize $\Delta X_b^2(\theta,T)$.
2. Optimize and update Ω and ϕ.
End While
Return: Variance $\Delta X_b^2(\theta,t)$, driving amplitude Ω, and phase ϕ.

$X_b(\theta,t)\equiv X_b(t)\cos\theta+Y_b(t)\sin\theta$ (θ is the squeezing angle). The variance of the rotating-quadrature operator is given by

$$\Delta X_b^2(\theta,t)=\mathbf{V}_{33}(t)\cos^2\theta+\mathbf{V}_{44}(t)\sin^2\theta+\tfrac{1}{2}[\mathbf{V}_{34}(t)+\mathbf{V}_{43}(t)]\sin(2\theta). \tag{12}$$

Based on $[X_b(\theta,t),X_b(\theta+\pi,t)]=i$, we have $\Delta X_b^2(\theta,t)\,\Delta X_b^2(\theta+\pi,t)\geqslant 1/4$, then the quadrature squeezing of the mechanical mode occurs when $\Delta X_b^2(\theta,t)<1/2$. For the squeezing-generation task, our goal is to reduce the variance $\Delta X_b^2(\theta,t)$ such that it is smaller than $1/2$. The control strategy of squeezing generation is summarized in Algorithm 1. Note that a variable learning rate method is adopted here to reduce the iteration number and to improve the efficiency. The detailed calculation of $\delta[\Delta X_b^2(\theta,T)]/\delta\mathcal{Q}_m$ is shown in the Appendix.

The mechanical quadrature squeezing can be well quantized by the squeezing degree [39]:

$$\mathcal{S}_b=-10\log_{10}\frac{\Delta X_b^2(\theta,t)}{\Delta X_b^2(\theta)|_{\rm ZPF}}. \tag{13}$$

A positive squeezing degree, $\mathcal{S}_b>0$, implies that the quadrature operator of the mechanical mode is squeezed along the angle θ. For studying the rotating-quadrature squeezing, we need to investigate the dependence of the squeezing on the angle θ. Concretely, we use the gradient-descent algorithm to obtain the waveforms of the driving amplitude and phase corresponding to $\mathcal{S}_b=1$ at different values of θ. The results shown in Fig. 1(a) indicate that the smallest (largest) driving amplitude appears at the squeezing angle 90° (0°) related to

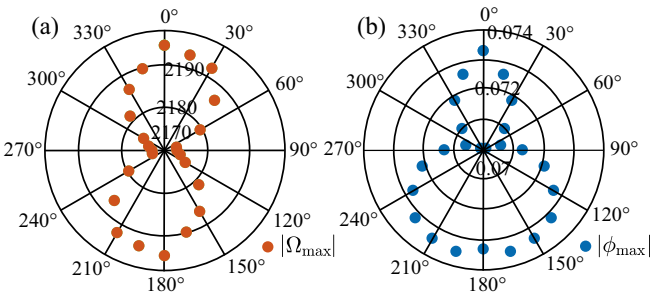

FIG. 1. Maximal absolute values of (a) the driving amplitude and (b) phase as functions of squeezing angle θ when the squeezing degree $\mathcal{S}_b=1$. Here, the parameters used are $g_0/\omega_{\rm m}=4\times10^{-5}$, $\kappa/\omega_{\rm m}=0.2$, $\gamma/\omega_{\rm m}=2\times10^{-6}$, $T=120\omega_{\rm m}^{-1}$, $\bar{n}_{\rm m}=100$, and $\Delta_{\rm c}/\omega_{\rm m}=1$.

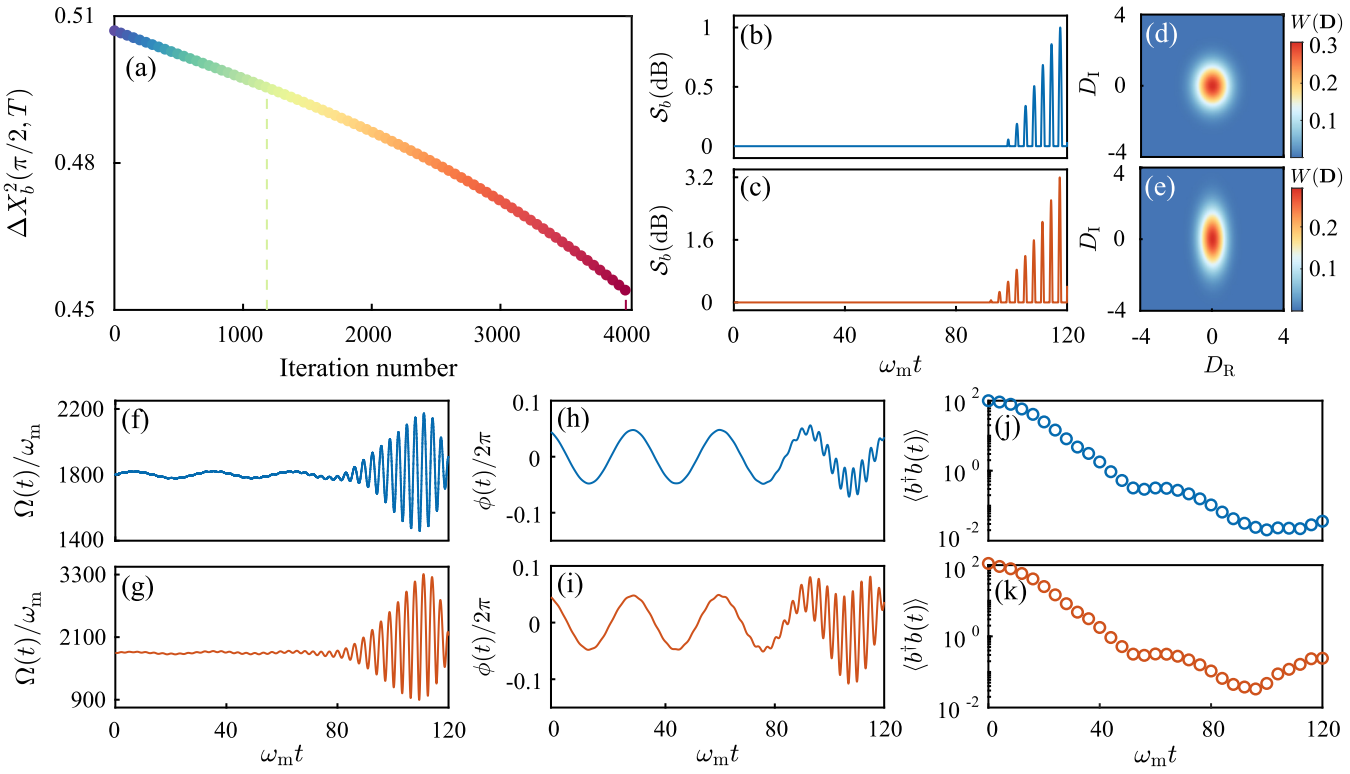

FIG. 2. (a) The loss function $\Delta X_b^2(\theta = \pi/2, T)$ as a function of the iteration number. The squeezing degree $\mathcal{S}_b$ vs the scaled evolution time $\omega_m t$ under different target squeezing degrees: (b) $\mathcal{S}_b = 1$ and (c) $\mathcal{S}_b = 3.2$. (d), (e) The Wigner functions of the generated states for the mechanical mode corresponding to the maximal squeezing in panels (b) and (c). (f), (g) The scaled driving amplitude $\Omega(t)/\omega_m$, (h), (i) phase $\phi(t)/2\pi$, and (j), (k) mean phonon number $\langle b^\dagger b\rangle$ as functions of the scaled evolution time $\omega_m t$ corresponding to panels (b) and (c). Other parameters used are the same as those given in Fig. 1.

$\mathcal{S}_b = 1$. Similarly, the minimal and maximal driving phases appear at 65° and 165°, respectively, and the angle has little effect on the phase [as shown in Fig. 1(b)]. Therefore, we take the squeezing angle $\theta = 90°$ (corresponding to minimal driving amplitude) in our following discussions.

We display in Fig. 2(a) the loss function $\Delta X_b^2(\pi/2, T)$ as a function of the iteration number to verify the efficiency of the gradient-descent algorithm. Here, we can see that the loss function $\Delta X_b^2(\pi/2, T)$ decreases gradually as the iteration number increases. The transient mechanical squeezing degrees 1 and 3.2 dB are obtained at the iteration numbers 1185 and 4000, respectively. The corresponding dynamic evolutions of the squeezing degree $\mathcal{S}_b$ are shown in Figs. 2(b) and 2(c). It shows that there is no mechanical squeezing for a long duration of time, first, and then oscillation increases to the target value in a short period of time. In particular, the squeezing degree $\mathcal{S}_b = 3.2$ breaks the 3-dB steady-state limit [Fig. 2(c)], and stronger squeezings can be realized as the iteration number increases. Note that we consider the transient squeezing here rather than steady-state squeezing. Therefore, our results are not conflicting with the 3-dB steady-state squeezing limit, which is determined by the dynamic stability.

To confirm the mechanical squeezing in phase space, we introduce the Wigner function of the mechanical mode, defined as [63]

$$W(\mathbf{D}) = \frac{1}{2\pi\sqrt{\mathrm{Det}[\mathbf{V}_b]}} \exp\left\{-\frac{1}{2}\mathbf{D}^{\mathrm{T}}\mathbf{V}_b\mathbf{D}\right\}, \tag{14}$$

where $\mathbf{D} = (D_R, D_I)^{\mathrm{T}}$ represents the two-dimensional vector, and $\mathbf{V}_b$ is the covariance matrix for the mechanical mode. The Wigner functions corresponding to 1- and 3.2-dB squeezing are shown in Figs. 2(d) and 2(e). We can see that the squeezing appears along the $\pi/2$ axis (corresponding to the squeezing angle $\theta = \pi/2$), and the larger the squeezing degree the stronger the quadrature squeezing.

In Figs. 2(f) and 2(g), we show the time-dependent driving amplitudes, which are required to achieve the squeezing degrees $\mathcal{S}_b = 1$ and 3.2 dB, respectively [64]. We can see that a larger driving amplitude is required to realize a stronger squeezing. In addition, for a larger mechanical squeezing degree, the driving phase oscillation becomes more intense, as shown in Figs. 2(h) and 2(i). We also investigate the dependence of the mean phonon number $\langle b^\dagger b\rangle$ (in the displaced representation, associated with the quantum fluctuation) as a function of the scaled time $\omega_m t$ in Figs. 2(j) and 2(k). We observe that $\langle b^\dagger b\rangle$ decreases from 100 to less than 1 for both $\mathcal{S}_b = 1$ and 3.2 dB. Note that in our simulations, the mechanical resonator is assumed initially in a thermal state at the same temperature with the heat bath. The density matrix for the thermal state is given by $\rho_{\mathrm{th}} = \sum_{n=0}^{\infty} P_n|n\rangle\langle n|$, where $P_n = \bar{n}_{\mathrm{th}}^n/(\bar{n}_{\mathrm{th}}+1)^{n+1}$ represents the probability distribution, with the mean thermal phonon number $\bar{n}_{\mathrm{th}} = \mathrm{Tr}(\rho_{\mathrm{th}} b^\dagger b) = 1/(e^{\hbar\omega_m/k_B T} - 1)$.

To explore the influence of the deviations in $\Omega(t)$ and $\phi(t)$ on mechanical quadrature squeezing, we introduce the

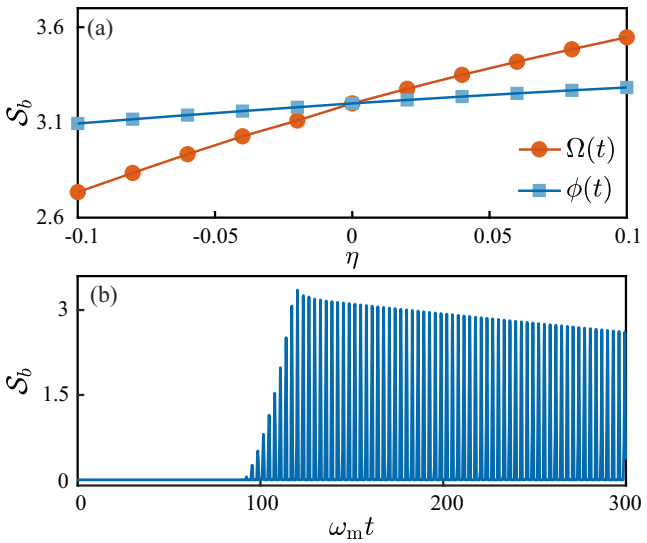

FIG. 3. (a) The influence of the driving amplitude and phase deviations on the squeezing generation at $T = 120\omega_m^{-1}$ related to $\mathcal{S}_b = 3.2$. (b) The dynamic evolution of the squeezing degree $\mathcal{S}_b$ after removing the pulsed driving in Fig. 2(c). Other parameters used are consistent with those given in Fig. 1.

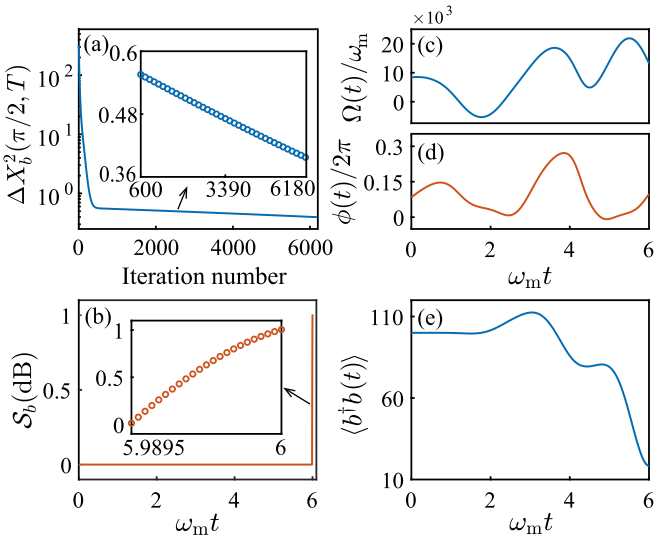

FIG. 4. (a) The loss function $\Delta X_b^2(\pi/2, T)$ as a function of the iteration number under $T = 6\omega_m^{-1}$. The inset shows the local magnification of the loss function over the iteration interval [600,6180]. (b) Evolution of the squeezing degree $\mathcal{S}_b$ in one mechanical oscillation period. The inset shows the evolution of $\mathcal{S}_b$ over time duration [5.9895,6]. (c) The driving amplitude $\Omega(t)/\omega_m$ and (d) phase $\phi(t)/2\pi$ vs the scaled evolution time $\omega_m t$ after the last iteration ($m = 6180$) under $T = 6\omega_m^{-1}$. (e) The mean phonon number $\langle b^\dagger b\rangle$ as a function of the scaled evolution time $\omega_m t$ corresponding to panel (b). Other parameters used are the same as those given in Fig. 1.

relative deviation η, defined as $\eta = (Q_r - Q_t)/Q_t$. Here Q represents either Ω or ϕ, and Q_r and Q_t stand for the realistically used parameters and the learned theoretical parameters, respectively. In Fig. 3(a), we plot the squeezing degree $\mathcal{S}_b$ as a function of η. Here, we see that for the relative deviation $\eta \in [-0.1, 0.1]$, the $\mathcal{S}_b$ is an increasing function of η for both the driving amplitude and phase. In addition, the squeezing is more sensitive to amplitude deviation than phase deviation. In Fig. 3(b), we further investigate the influence of the environment on the squeezing generation once the pulsed driving is removed at $T = 120\omega_m^{-1}$. The $\mathcal{S}_b$ will experience a slight decrease from 3.2 to 2.51 during the period from $\omega_m t = 120$ to 300, indicating that the squeezing has a good robustness. Notably, after the external drive is removed, the photons in the cavity will dissipate completely within a certain period, and the optomechanical interaction will no longer work. Consequently, the mechanical resonator will be thermalized by the heat bath, leading to a reduction of the mechanical quadrature squeezing.

The ultrafast generation of mechanical quadrature squeezing within one mechanical oscillation period is a desired task from the viewpoint of transient evolution [65,66]. Below, we investigate the generation of mechanical squeezing within this short timescale. Figure 4(a) shows the loss function $\Delta X_b^2(\pi/2, T = 6\omega_m^{-1})$ versus the iteration number related to $\mathcal{S}_b = 1$. Here we can see that the $\Delta X_b^2(\pi/2, T = 6\omega_m^{-1})$ gradually decreases from the initial value 319 to 0.397 as the iteration number increases, verifying the validity of the gradient-descent algorithm. The dynamic evolution of the squeezing degree $\mathcal{S}_b$ after the last iteration ($m = 6180$) is shown in Fig. 4(b). We see that the squeezing occurs in the last extremely short duration due to the harsh time condition, but it is still continuous, as shown in the inset of Fig. 4(b). The results in Figs. 4(c) and 4(d) indicate that a large driving amplitude is required to achieve $\mathcal{S}_b = 1$ within one mechanical oscillation period and the phase has no distinct signature. We also exhibit in Fig. 4(e) the mean phonon number $\langle b^\dagger b\rangle$ versus the scaled evolution time at this time. Here we see that $\langle b^\dagger b\rangle$ will be larger than the initial value due to the larger driving amplitude, and then goes to a cooled state with dozens of mean phonons. This indicates that the creation of mechanical squeezing does not necessarily require the ground-state cooling of the mechanical resonator.

We also investigate the influence of the sideband-resolution parameter on the squeezing generation. In Figs. 5(a)–5(c), we plot the squeezing degree $\mathcal{S}_b$ versus the scaled evolution time $\omega_m t$ corresponding to different sideband-resolution parameters $\kappa/\omega_m = 0.5$, 1.0, and 1.5. We show the driving amplitude and phase as functions of $\omega_m t$ for different sideband-resolution parameters in Figs. 5(d)–5(f) and 5(g)–5(i). To maintain $\mathcal{S}_b = 1$, a larger driving amplitude is needed for a larger value of κ/ω_m, and the phase oscillation becomes more severe for a larger κ/ω_m. The corresponding dynamic evolution of the mean phonon number $\langle b^\dagger b\rangle$ is shown in Fig. 5(j). Here we can see that the mechanical resonator is cooled from the initial 100 phonons to a few phonons. The better the sideband-resolution parameter that is is selected, the deeper the cooling of the mechanical resonator. Note that a large κ/ω_m will result in a fast dissipation of the cavity photons, thereby affecting the optomechanical interaction and leading to the failure of squeezing generation. We mention that the thermal excitations are usually harmful to the generation and maintenance of quantum signatures. For the generation of strong quadrature squeezing, optimal parameters should be chosen such that the thermal excitations can be decreased to a near-ground-state cooling level.

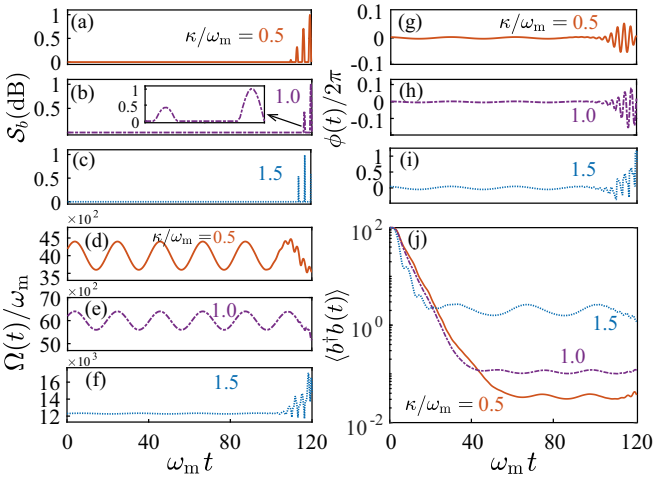

FIG. 5. (a)–(c) The squeezing degree $\mathcal{S}_b$ vs the scaled evolution time $\omega_m t$ under different sideband parameters $\kappa/\omega_m = 0.5$, 1.0, and 1.5. The inset in panel (b) exhibits the evolution of $\mathcal{S}_b$ for the time durations from 115.6 to 120. (d)–(f) Evolution of driving amplitude and (g)–(i) phase corresponding to panels (a)–(c). (j) The dynamic evolution of the mean phonon number under different sideband-resolution parameters in panels (a)–(c). The two insets show the enlarged view at the peak of 3.2 dB. Other parameters are consistent with those given in Fig. 1.

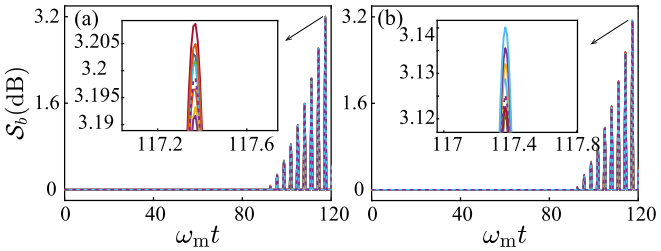

FIG. 6. The squeezing degree $\mathcal{S}_b$ vs the scaled evolution time $\omega_m t$ in the presence of (a) driving amplitude and (b) phase noises. The driving amplitude is modified by adding a scaled random amplitude from a normal distribution with a mean of zero and a standard deviation of 200. Similarly, the driving phase is modified by adding a scaled random phase from a normal distribution with a mean of zero and a standard deviation of 0.2. Other parameters are the same as those in Fig. 2(c).

IV. DISCUSSIONS

In this section, we present some discussions concerning the influences of the driving amplitude and phase noises on the squeezing generation, the physical mechanism of the present squeezing-generation method, the experimental implementation of this scheme, and the applications of the optimization methods in cavity optomechanics.

A. Influences of the driving amplitude and phase noises on squeezing generation

In realistic situations, the driving laser inevitably possesses amplitude and phase noises, which can be understood as random small deviations on the amplitude and phase. To evaluate the influences of laser amplitude and phase noises on the squeezing-generation performance, we add Gaussian random noises to the optimized pulse driving amplitude and phase at each step. Figures 6(a) and 6(b) display the squeezing degree $\mathcal{S}_b$ as a function of the scaled evolution time $\omega_m t$ after introducing the Gaussian random noises to the driving amplitude and phase, respectively. The ten solid curves represent the evolution of the squeezing degree $\mathcal{S}_b$ under ten distinct random conditions, while the purple dotted curve represents the average of these ten evolutions. We can see that the 11 curves almost overlap, which indicates that the optimized driving field is stable against both the amplitude and phase noises.

B. Physical mechanism of the present squeezing-generation method

In our scheme, the generation of mechanical squeezing can be understood by analyzing the variance of the mechanical rotating-quadrature operator $\Delta X_b^2(\theta,t) = \mathbf{V}_{33}(t)\cos^2\theta + \mathbf{V}_{44}(t)\sin^2\theta + \frac{1}{2}[\mathbf{V}_{34}(t) + \mathbf{V}_{43}(t)]\sin(2\theta)$. To clarify this point, we reexpress the rotating-quadrature operator as

$$\Delta X_b^2(\theta,t) = \tfrac{1}{2} + \langle b^\dagger b\rangle + \mathrm{Re}[\langle b^\dagger b^\dagger\rangle]\cos(2\theta) - 2\mathrm{Im}[\langle b^\dagger b^\dagger\rangle]\sin(2\theta). \quad (15)$$

Mechanical squeezing occurs when $\Delta X_b^2(\theta,t) < 1/2$, which leads to the condition

$$\langle b^\dagger b\rangle + \mathrm{Re}[\langle b^\dagger b^\dagger\rangle]\cos(2\theta) - 2\mathrm{Im}[\langle b^\dagger b^\dagger\rangle]\sin(2\theta) < 0. \quad (16)$$

This inequality can be satisfied because the second-order moment $\langle b^\dagger b^\dagger\rangle$ could be a complex number, while $\langle b^\dagger b\rangle$ must be positive. Our numerical simulations indicate the mechanical cooling is accompanied by the physics process, and the mechanical resonator is cooled to a relatively small mean phonon number [Figs. 2(j), 2(k), 4(e), and 5(j)]. Therefore, the generation of the mechanical squeezing is primarily determined by the values of $\mathrm{Re}[\langle b^\dagger b^\dagger\rangle]$ and $\mathrm{Im}[\langle b^\dagger b^\dagger\rangle]$.

Under the rotating-wave approximation, the second-order moments are governed by two separate sets of equations. The first set includes $\langle a^\dagger a\rangle$, $\langle b^\dagger b\rangle$, $\langle a^\dagger b\rangle$, and $\langle ab^\dagger\rangle$, while the second set includes $\langle a^\dagger a^\dagger\rangle$, $\langle aa\rangle$, $\langle b^\dagger b^\dagger\rangle$, $\langle bb\rangle$, $\langle a^\dagger b^\dagger\rangle$, and $\langle ab\rangle$. With the initial condition $\mathbf{X}(0) = [0, \bar{n}_m, 0, 0, 0, 0, 0, 0, 0, 0]^T$, the value of $\langle b^\dagger b^\dagger\rangle$ remains constantly zero, leading to a negligible mechanical squeezing regardless of how we optimize the driving fields. The counter-rotating terms in the coupling will mix the equations of motion for these ten second-order moments. In this case, we can obtain $\langle b^\dagger b\rangle + \mathrm{Re}[\langle b^\dagger b^\dagger\rangle]\cos(2\theta) - 2\mathrm{Im}[\langle b^\dagger b^\dagger\rangle]\sin(2\theta) < 0$ via optimizing the pulsed driving, indicating the generation of squeezing. These analyses indicate that the critical role of the counter-rotating terms is the generation of mechanical quadrature squeezing.

Meanwhile, we examined the single-mode squeezing properties of the two-mode squeezed vacuum state and the state obtained by applying the two-mode squeezing operator to the direct product of vacuum and thermal states. We find

that there is no single-mode quadrature squeezing in these two cases, indicating that the pure counter-rotating-wave terms are insufficient for generating single-mode squeezing. Based on these analyses, we deduce that the generation of single-mode quadrature squeezing arises from the combined effects of both rotating-wave and counter-rotating-wave terms. Since both the linearized optomechanical-coupling strength $G(t)$ and the normalized driving detuning $\Delta(t)$ depend on the evolution time, these provide the possibility to induce the physical process for effective two-phonon interactions, which is the physical origin for generating single-mode squeezing.

C. Experimental implementation of the scheme

We now present some discussions on the experimental feasibility of this scheme. The system under considerations is a general optomechanical system, which has been implemented in various optomechanical platforms, such as optical microresonators [67–69], electromechanical systems [70–72], photonic crystal nanobeams [5,73,74], and Fabry-Pérot cavities [75], in which the cavities can be driven by tunable pulsed fields. We considered the linearized optomechanical interaction, which has been widely demonstrated in cavity optomechanical systems. Moreover, we use the experimentally accessible parameters in our numerical simulations. Concretely, the used parameters are $g_0/\omega_{\rm m} = 4 \times 10^{-5}$, $\kappa/\omega_{\rm m} = 0.2$, and $\gamma/\omega_{\rm m} = 2 \times 10^{-6}$, which have been reported in experiments [69]. In addition, the pulsed driving amplitude and phase used to generate squeezing are moderate in size and continuous and smooth in shape, which confirm the experimental realization of the pulsed driving.

D. Applications of the optimization methods in cavity optomechanics

To broaden the use of our optimization method in the field of cavity optomechanics, we investigate its applicability across two primary research regimes: the strong driving linearization regime and the single-photon strong-coupling regime.

In the strong driving linearization regime, the physical properties of the optomechanical system are governed by the covariance matrix. For this linearized optomechanical system, we can control the dynamics of the system by optimizing the driving field, which is an adjustable control parameter. For example, we can optimize the physical topics such as optomechanical cooling, entanglement, and squeezing. Moreover, this optimization problem can be extended and applied to multimode optomechanical systems.

In the single-photon strong-coupling regime, the optomechanical system can be described as a multilevel system in the eigenrepresentation of the photon-number-dependent displaced oscillator system. The driving field will induce the transitions between the states associated with neighboring photon numbers. Here, the transition magnitudes depend on the external driving field, which provide the means for controlling the systems. Typically, the optimization allows for several potential applications, including the enhancement of the photon-blockade effect and the preparation of nonclassical states such as mechanical number states. By implementing these optimizations, we can deepen both the understanding and the practical applications of the cavity optomechanical systems.

V. CONCLUSION

In conclusion, we have presented a scheme for generating mechanical quadrature squeezing in a typical optomechanical system via gradient-descent algorithm. The generated mechanical squeezing can exceed the 3-dB steady-state limit and ultrafast squeezing preparation within one mechanical oscillation period can be realized. The optimal driving amplitude and phase corresponding to these generated squeezings have been presented. Our scheme will pave the way for exploiting optimal quantum control in quantum optics and quantum information science.

ACKNOWLEDGMENTS

The authors thank Dr. Y.-X. Zeng and Dr. Y.-H. Zhou for helpful discussions. J.-Q.L. was supported in part by National Natural Science Foundation of China (Grants No. 12175061, No. 12247105, and No. 11935006), National Key Research and Development Program of China (Grant No. 2024YFE0102400), and Hunan Provincial Major Sci-Tech Program (Grant No. 2023ZJ1010). Y.-H.L. was supported in part by Hunan Provincial Postgraduate Research and Innovation project (Grant No. CX20240530).

APPENDIX: DERIVATION OF THE VARIATION $\delta[\Delta X_b^2(\theta, T)]/\delta\mathcal{Q}_m$

For generation of mechanical quadrature squeezing, we need to minimize the loss function $\Delta X_b^2(\theta, T)$. In this Appendix, we will clarify in detail how to achieve this goal using the gradient-descent algorithm. The mathematical expression of the gradient-descent algorithm for mechanical squeezing generation is

$$\mathcal{Q}_{m+1} = \mathcal{Q}_m - \chi_{\mathcal{Q}} \frac{\delta\left[\Delta X_b^2(\theta, T)\right]}{\delta \mathcal{Q}_m}, \tag{A1}$$

where $\mathcal{Q}$ could be either Ω or ϕ, m is the iteration number, and $\chi_{\mathcal{Q}}$ is the learning rate. To calculate Eq. (A1), we need to calculate the variation of $\Delta X_b^2(\theta, T)$ with respect to the pulse amplitude $\Omega(s)$ and phase $\phi(s)$. Based on Eq. (12), we can obtain the result

$$\frac{\delta \Delta X_b^2(\theta, T)}{\delta \mathcal{Q}(s)} = \frac{\delta \mathrm{V}_{33}(T)}{\delta \mathcal{Q}(s)} \cos^2\theta + \frac{\delta \mathrm{V}_{44}(T)}{\delta \mathcal{Q}(s)} \sin^2\theta + \left[\frac{\delta \mathrm{V}_{34}(T)}{\delta \mathcal{Q}(s)} + \frac{\delta \mathrm{V}_{43}(T)}{\delta \mathcal{Q}(s)}\right] \sin(2\theta). \tag{A2}$$

According to Eq. (A2), we can further calculate the results of $\delta \mathrm{V}_{33}(T)/\delta\mathcal{Q}(s)$, $\delta \mathrm{V}_{44}(T)/\delta\mathcal{Q}(s)$, $\delta \mathrm{V}_{34}(T)/\delta\mathcal{Q}(s)$, and $\delta \mathrm{V}_{43}(T)/\delta\mathcal{Q}(s)$. The variation of the covariance-matrix elements with respect to the pulse amplitude $\Omega(s)$ and phase $\phi(s)$ can be expressed as a linear combination of the variation of these second-order moments with respect to the

driving amplitude $\Omega(s)$ and phase $\phi(s)$:

$$\frac{\delta \mathbf{V}_{11}(T)}{\delta \mathcal{Q}(s)} = \frac{1}{2}\frac{\delta\langle a^\dagger a^\dagger(T)\rangle}{\delta \mathcal{Q}(s)} + \frac{\delta\langle a^\dagger a(T)\rangle}{\delta \mathcal{Q}(s)} + \frac{1}{2}\frac{\delta\langle aa(T)\rangle}{\delta \mathcal{Q}(s)}, \tag{A3a}$$

$$\frac{\delta \mathbf{V}_{12}(T)}{\delta \mathcal{Q}(s)} = \frac{i}{2}\frac{\delta\langle a^\dagger a^\dagger(T)\rangle}{\delta \mathcal{Q}(s)} - \frac{i}{2}\frac{\delta\langle aa(T)\rangle}{\delta \mathcal{Q}(s)}, \tag{A3b}$$

$$\frac{\delta \mathbf{V}_{13}(T)}{\delta \mathcal{Q}(s)} = \frac{1}{2}\frac{\delta\langle a^\dagger b^\dagger(T)\rangle}{\delta \mathcal{Q}(s)} + \frac{1}{2}\frac{\delta\langle a^\dagger b(T)\rangle}{\delta \mathcal{Q}(s)} + \frac{1}{2}\frac{\delta\langle ab^\dagger(T)\rangle}{\delta \mathcal{Q}(s)} + \frac{1}{2}\frac{\delta\langle ab(T)\rangle}{\delta \mathcal{Q}(s)}, \tag{A3c}$$

$$\frac{\delta \mathbf{V}_{14}(T)}{\delta \mathcal{Q}(s)} = \frac{i}{2}\frac{\delta\langle a^\dagger b^\dagger(T)\rangle}{\delta \mathcal{Q}(s)} - \frac{i}{2}\frac{\delta\langle a^\dagger b(T)\rangle}{\delta \mathcal{Q}(s)} + \frac{i}{2}\frac{\delta\langle ab^\dagger(T)\rangle}{\delta \mathcal{Q}(s)} - \frac{i}{2}\frac{\delta\langle ab(T)\rangle}{\delta \mathcal{Q}(s)}, \tag{A3d}$$

$$\frac{\delta \mathbf{V}_{22}(T)}{\delta \mathcal{Q}(s)} = -\frac{1}{2}\frac{\delta\langle a^\dagger a^\dagger(T)\rangle}{\delta \mathcal{Q}(s)} + \frac{\delta\langle a^\dagger a(T)\rangle}{\delta \mathcal{Q}(s)} - \frac{1}{2}\frac{\delta\langle aa(T)\rangle}{\delta \mathcal{Q}(s)}, \tag{A3e}$$

$$\frac{\delta \mathbf{V}_{23}(T)}{\delta \mathcal{Q}(s)} = \frac{i}{2}\frac{\delta\langle a^\dagger b^\dagger(T)\rangle}{\delta \mathcal{Q}(s)} + \frac{i}{2}\frac{\delta\langle a^\dagger b(T)\rangle}{\delta \mathcal{Q}(s)} - \frac{i}{2}\frac{\delta\langle ab^\dagger(T)\rangle}{\delta \mathcal{Q}(s)} - \frac{i}{2}\frac{\delta\langle ab(T)\rangle}{\delta \mathcal{Q}(s)}, \tag{A3f}$$

$$\frac{\delta \mathbf{V}_{24}(T)}{\delta \mathcal{Q}(s)} = -\frac{1}{2}\frac{\delta\langle a^\dagger b^\dagger(T)\rangle}{\delta \mathcal{Q}(s)} + \frac{1}{2}\frac{\delta\langle a^\dagger b(T)\rangle}{\delta \mathcal{Q}(s)} + \frac{1}{2}\frac{\delta\langle ab^\dagger(T)\rangle}{\delta \mathcal{Q}(s)} - \frac{1}{2}\frac{\delta\langle ab(T)\rangle}{\delta \mathcal{Q}(s)}, \tag{A3g}$$

$$\frac{\delta \mathbf{V}_{33}(T)}{\delta \mathcal{Q}(s)} = \frac{1}{2}\frac{\delta\langle b^\dagger b^\dagger(T)\rangle}{\delta \mathcal{Q}(s)} + \frac{\delta\langle b^\dagger b(T)\rangle}{\delta \mathcal{Q}(s)} + \frac{1}{2}\frac{\delta\langle bb(T)\rangle}{\delta \mathcal{Q}(s)}, \tag{A3h}$$

$$\frac{\delta \mathbf{V}_{34}(T)}{\delta \mathcal{Q}(s)} = \frac{i}{2}\frac{\delta\langle b^\dagger b^\dagger(T)\rangle}{\delta \mathcal{Q}(s)} - \frac{i}{2}\frac{\delta\langle bb(T)\rangle}{\delta \mathcal{Q}(s)}, \tag{A3i}$$

$$\frac{\delta \mathbf{V}_{44}(T)}{\delta \mathcal{Q}(s)} = -\frac{1}{2}\frac{\delta\langle b^\dagger b^\dagger(T)\rangle}{\delta \mathcal{Q}(s)} + \frac{\delta\langle b^\dagger b(T)\rangle}{\delta \mathcal{Q}(s)} - \frac{1}{2}\frac{\delta\langle bb(T)\rangle}{\delta \mathcal{Q}(s)}. \tag{A3j}$$

The variation for other covariance-matrix elements can be obtained based on the Hermitian conjugate relations.

It can be seen from Eq. (A3) that, to obtain the result in Eq. (A2), we need to further calculate the variations of these second-order moments with respect to $\Omega(s)$ and $\phi(s)$. This can be achieved by taking the variation with respect to $\Omega(s)$ and $\phi(s)$ on both sides of Eq. (8), namely,

$$\frac{\delta \dot{\mathbf{X}}(t)}{\delta \mathcal{Q}(s)} = \mathbf{M}(t)\frac{\delta \mathbf{X}(t)}{\delta \mathcal{Q}(s)} + \frac{\delta \mathbf{M}(t)}{\delta \mathcal{Q}(s)}\mathbf{X}(t) + \frac{\delta \mathbf{N}(t)}{\delta \mathcal{Q}(s)}. \tag{A4}$$

Since $\mathcal{Q}(s)$ is a function of s, $\delta\dot{\mathbf{X}}(t)/\delta\mathcal{Q}(s)$ in Eq. (A4) can be expressed as $\frac{d}{dt}\frac{\delta \mathbf{X}(t)}{\delta \mathcal{Q}(s)}$ [76]. Under the initial condition $\delta\mathbf{X}(0)/\delta\mathcal{Q}(s) = [0, \ldots, 0]^{\mathrm{T}}_{10\times 1}$, the solution of Eq. (A4) at the target time T can be obtained as

$$\begin{aligned}\frac{\delta \mathbf{X}(T)}{\delta \mathcal{Q}(s)} &= \mathbf{U}(T)\frac{\delta \mathbf{X}(0)}{\delta \mathcal{Q}(s)} + \mathbf{U}(T)\int_0^T d\tau \mathbf{U}^{-1}(\tau)\left[\frac{\delta \mathbf{M}(\tau)}{\delta \mathcal{Q}(s)}\mathbf{X}(\tau) + \frac{\delta \mathbf{N}(\tau)}{\delta \mathcal{Q}(s)}\right] \\ &= \mathbf{U}(T)\int_0^T d\tau \mathbf{U}^{-1}(\tau)\left[\frac{\delta \mathbf{M}(\tau)}{\delta \mathcal{Q}(\tau)}\frac{\delta \mathcal{Q}(\tau)}{\delta \mathcal{Q}(s)}\mathbf{X}(\tau) + \frac{\delta \mathbf{N}(\tau)}{\delta \mathcal{Q}(\tau)}\frac{\delta \mathcal{Q}(\tau)}{\delta \mathcal{Q}(s)}\right] \\ &= \mathbf{U}(T)\mathbf{U}^{-1}(s)\left[\frac{\delta \mathbf{M}(s)}{\delta \mathcal{Q}(s)}\mathbf{X}(s) + \frac{\delta \mathbf{N}(s)}{\delta \mathcal{Q}(s)}\right],\end{aligned} \tag{A5}$$

where $\mathbf{U}(t)$ satisfies $\dot{\mathbf{U}}(t) = \mathbf{M}(t)\mathbf{U}(t)$ with the initial value $\mathbf{U}(0) = I$.

To know the explicit expressions for $\delta\mathbf{M}(s)/\delta\mathcal{Q}(s)$ and $\delta\mathbf{N}(s)/\delta\mathcal{Q}(s)$ in Eq. (A5), we need to obtain the values of $\delta\alpha(s)/\delta\mathcal{Q}(s)$, $\delta\beta(s)/\delta\mathcal{Q}(s)$, and their Hermitian conjugate. Taking the variation with respect to $\mathcal{Q}(s)$ on both sides of Eqs. (6a) and (6b) as well as their Hermitian conjugate equations, we have

$$\dot{\mathbf{A}}(t) = \mathbf{W}(t)\mathbf{A}(t) + \mathbf{Q}(t), \tag{A6}$$

where

$$\mathbf{A}(t) = \left(\frac{\delta\alpha(t)}{\delta \mathcal{Q}(s)}, \frac{\delta\beta(t)}{\delta \mathcal{Q}(s)}, \frac{\delta\alpha^*(t)}{\delta \mathcal{Q}(s)}, \frac{\delta\beta^*(t)}{\delta \mathcal{Q}(s)}\right)^{\mathrm{T}}, \tag{A7}$$

$$\mathbf{W}(t)=\begin{pmatrix} -i\Delta(t)-\frac{\kappa}{2} & 0 & -ig_0\alpha & -ig_0\alpha \\ -ig_0\alpha^* & -ig_0\alpha & -i\omega_{\mathrm{m}}-\frac{\gamma}{2} & 0 \\ 0 & i\Delta(t)-\frac{\kappa}{2} & ig_0\alpha^* & ig_0\alpha^* \\ ig_0\alpha^* & ig_0\alpha & 0 & i\omega_{\mathrm{m}}-\frac{\gamma}{2} \end{pmatrix}, \tag{A8}$$

and

$$\mathbf{Q}(t)=\begin{pmatrix} i\frac{\delta\Omega(t)}{\delta\mathcal{Q}(s)}e^{-i\phi(t)}+i\Omega(t)\frac{\delta[e^{-i\phi(t)}]}{\delta\mathcal{Q}(s)} \\ 0 \\ -i\frac{\delta\Omega(t)}{\delta\mathcal{Q}(s)}e^{i\phi(t)}-i\Omega(t)\frac{\delta[e^{i\phi(t)}]}{\delta\mathcal{Q}(s)} \\ 0 \end{pmatrix}. \tag{A9}$$

The solution to Eq. (A6) can be expressed as

$$\mathbf{A}(t)=\Lambda(t)\mathbf{A}(0)+\Lambda(t)\int_0^t\Lambda^{-1}(\tau)\mathbf{Q}(\tau)d\tau, \tag{A10}$$

where $\mathbf{A}(0)=[0,0,0,0]^{\mathrm{T}}$ and $\Lambda(t)$ satisfies the equation $\dot{\Lambda}(t)=\mathbf{W}(t)\Lambda(t)$ with the initial value $\Lambda(0)=I$. Then, we have

$$\left(\frac{\delta\alpha(s)}{\delta\Omega(s)},\frac{\delta\beta(s)}{\delta\Omega(s)},\frac{\delta\alpha^*(s)}{\delta\Omega(s)},\frac{\delta\beta^*(s)}{\delta\Omega(s)}\right)^{\mathrm{T}}=\left(\frac{1}{2}ie^{-i\phi(s)},0,-\frac{1}{2}ie^{i\phi(s)},0\right)^{\mathrm{T}}, \tag{A11a}$$

$$\left(\frac{\delta\alpha(s)}{\delta\phi(s)},\frac{\delta\beta(s)}{\delta\phi(s)},\frac{\delta\alpha^*(s)}{\delta\phi(s)},\frac{\delta\beta^*(s)}{\delta\phi(s)}\right)^{\mathrm{T}}=\left(\frac{1}{2}\Omega(s)e^{-i\phi(s)},0,\frac{1}{2}\Omega(s)e^{i\phi(s)},0\right)^{\mathrm{T}}. \tag{A11b}$$

Thus, we obtain the variation of the displacement amplitudes $\alpha(s)$ and $\beta(s)$ with respect to the driving amplitude $\Omega(s)$ and phase $\phi(s)$, respectively. Based on the value of $\delta[\Delta X_b^2(\theta,T)]/\delta\mathcal{Q}(s)$, we can further perform the gradient-descent algorithm until a satisfactory value of the loss function $\Delta X_b^2(\theta,T)$ is obtained.

[1] M. Aspelmeyer, T. J. Kippenberg, and F. Marquardt, Cavity optomechanics, Rev. Mod. Phys. **86**, 1391 (2014).

[2] I. Wilson-Rae, N. Nooshi, W. Zwerger, and T. J. Kippenberg, Theory of ground state cooling of a mechanical oscillator using dynamical backaction, Phys. Rev. Lett. **99**, 093901 (2007).

[3] F. Marquardt, J. P. Chen, A. A. Clerk, and S. M. Girvin, Quantum theory of cavity-assisted sideband cooling of mechanical motion, Phys. Rev. Lett. **99**, 093902 (2007).

[4] J. Chan, T. P. M. Alegre, A. H. Safavi-Naeini, J. T. Hill, A. Krause, S. Gröblacher, M. Aspelmeyer, and O. Painter, Laser cooling of a nanomechanical oscillator into its quantum ground state, Nature (London) **478**, 89 (2011).

[5] J. D. Teufel, T. Donner, D. Li, J. W. Harlow, M. S. Allman, K. Cicak, A. J. Sirois, J. D. Whittaker, K. W. Lehnert, and R. W. Simmonds, Sideband cooling of micromechanical motion to the quantum ground state, Nature (London) **475**, 359 (2011).

[6] D. Vitali, S. Gigan, A. Ferreira, H. R. Böhm, P. Tombesi, A. Guerreiro, V. Vedral, A. Zeilinger, and M. Aspelmeyer, Optomechanical entanglement between a movable mirror and a cavity field, Phys. Rev. Lett. **98**, 030405 (2007).

[7] T. A. Palomaki, J. D. Teufel, R. W. Simmonds, and K. W. Lehnert, Entangling mechanical motion with microwave fields, Science **342**, 710 (2013).

[8] R. Riedinger, S. Hong, R. A. Norte, J. A. Slater, J. Shang, A. G. Krause, V. Anant, M. Aspelmeyer, and S. Gröblacher, Non-classical correlations between single photons and phonons from a mechanical oscillator, Nature (London) **530**, 313 (2016).

[9] Y.-F. Jiao, S.-D. Zhang, Y.-L. Zhang, A. Miranowicz, L.-M. Kuang, and H. Jing, Nonreciprocal optomechanical entanglement against backscattering losses, Phys. Rev. Lett. **125**, 143605 (2020).

[10] H. Yu, L. McCuller, M. Tse, N. Kijbunchoo, L. Barsotti, N. Mavalvala, and L. S. Collaboration, Quantum correlations between light and the kilogram-mass mirrors of LIGO, Nature (London) **583**, 43 (2020).

[11] D.-G. Lai, J.-Q. Liao, A. Miranowicz, and F. Nori, Noise tolerant optomechanical entanglement via synthetic magnetism, Phys. Rev. Lett. **129**, 063602 (2022).

[12] S. Bose, K. Jacobs, and P. L. Knight, Preparation of nonclassical states in cavities with a moving mirror, Phys. Rev. A **56**, 4175 (1997).

[13] W. Marshall, C. Simon, R. Penrose, and D. Bouwmeester, Towards quantum superpositions of a mirror, Phys. Rev. Lett. **91**, 130401 (2003).

[14] J.-Q. Liao and L. Tian, Macroscopic quantum superposition in cavity optomechanics, Phys. Rev. Lett. **116**, 163602 (2016).

[15] J.-Q. Liao, J.-F. Huang, L. Tian, L.-Ma. Kuang, and C.-P. Sun, Generalized ultrastrong optomechanical-like coupling, Phys. Rev. A **101**, 063802 (2020).

[16] C. Fabre, M. Pinard, S. Bourzeix, A. Heidmann, E. Giacobino, and S. Reynaud, Quantum-noise reduction using a cavity with a movable mirror, Phys. Rev. A **49**, 1337 (1994).

[17] S. Mancini and P. Tombesi, Quantum noise reduction by radiation pressure, Phys. Rev. A **49**, 4055 (1994).

[18] D. W. C. Brooks, T. Botter, S. Schreppler, T. P. Purdy, N. Brahms, and D. M. Stamper-Kurn, Non-classical light generated by quantum-noise-driven cavity optomechanics, Nature (London) **488**, 476 (2012).

[19] T. P. Purdy, P.-L. Yu, R. W. Peterson, N. S. Kampel, and C. A. Regal, Strong optomechanical squeezing of light, Phys. Rev. X **3**, 031012 (2013).

[20] A. H. Safavi-Naeini, S. Gröblacher, J. T. Hill, J. Chan, M. Aspelmeyer, and O. Painter, Squeezed light from a silicon micromechanical resonator, Nature (London) **500**, 185 (2013).

[21] K. Qu and G. S. Agarwal, Strong squeezing via phonon mediated spontaneous generation of photon pairs, New J. Phys. **16**, 113004 (2014).

[22] M. J. Woolley, A. C. Doherty, G. J. Milburn, and K. C. Schwab, Nanomechanical squeezing with detection via a microwave cavity, Phys. Rev. A **78**, 062303 (2008).

[23] M. Rashid, T. Tufarelli, J. Bateman, J. Vovrosh, D. Hempston, M. S. Kim, and H. Ulbricht, Experimental realization of a thermal squeezed state of levitated optomechanics, Phys. Rev. Lett. **117**, 273601 (2016).

[24] J. Teufel, T. Donner, M. Castellanos-Beltran, J. Harlow, and K. Lehnert, Nanomechanical motion measured with an imprecision below that at the standard quantum limit, Nat. Nanotechnol. **4**, 820 (2009).

[25] A. Nunnenkamp, K. Børkje, J. G. E. Harris, and S. M. Girvin, Cooling and squeezing via quadratic optomechanical coupling, Phys. Rev. A **82**, 021806(R) (2010).

[26] J.-Q. Liao and C. K. Law, Parametric generation of quadrature squeezing of mirrors in cavity optomechanics, Phys. Rev. A **83**, 033820 (2011).

[27] G. Milburn and D. F. Walls, Production of squeezed states in a degenerate parametric amplifier, Opt. Commun. **39**, 401 (1981).

[28] A. Mari and J. Eisert, Gently modulating optomechanical systems, Phys. Rev. Lett. **103**, 213603 (2009).

[29] A. Pontin, M. Bonaldi, A. Borrielli, F. S. Cataliotti, F. Marino, G. A. Prodi, E. Serra, and F. Marin, Squeezing a thermal mechanical oscillator by stabilized parametric effect on the optical spring, Phys. Rev. Lett. **112**, 023601 (2014).

[30] A. Pontin, M. Bonaldi, A. Borrielli, L. Marconi, F. Marino, G. Pandraud, G. A. Prodi, P. M. Sarro, E. Serra, and F. Marin, Dynamical two-mode squeezing of thermal fluctuations in a cavity optomechanical system, Phys. Rev. Lett. **116**, 103601 (2016).

[31] A. Chowdhury, P. Vezio, M. Bonaldi, A. Borrielli, F. Marino, B. Morana, G. A. Prodi, P. M. Sarro, E. Serra, and F. Marin, Quantum signature of a squeezed mechanical oscillator, Phys. Rev. Lett. **124**, 023601 (2020).

[32] Y. Li, A.-N. Xu, L.-G. Huang, and Y.-C. Liu, Mechanical squeezing via detuning-switched driving, Phys. Rev. A **107**, 033508 (2023).

[33] A. A. Clerk, F. Marquardt, and K. Jacobs, Back-action evasion and squeezing of a mechanical resonator using a cavity detector, New J. Phys. **10**, 095010 (2008).

[34] A. Szorkovszky, A. C. Doherty, G. I. Harris, and W. P. Bowen, Mechanical squeezing via parametric amplification and weak measurement, Phys. Rev. Lett. **107**, 213603 (2011).

[35] G. Vasilakis, H. Shen, K. Jensen, M. Balabas, D. Salart, B. Chen, and E. S. Polzik, Generation of a squeezed state of an oscillator by stroboscopic back-action-evading measurement, Nat. Phys. **11**, 389 (2015).

[36] C. Meng, G. A. Brawley, J. S. Bennett, M. R. Vanner, and W. P. Bowen, Mechanical squeezing via fast continuous measurement, Phys. Rev. Lett. **125**, 043604 (2020).

[37] J.-M. Pirkkalainen, E. Damskägg, M. Brandt, F. Massel, and M. A. Sillanpää, Squeezing of quantum noise of motion in a micromechanical resonator, Phys. Rev. Lett. **115**, 243601 (2015).

[38] K. Jähne, C. Genes, K. Hammerer, M. Wallquist, E. S. Polzik, and P. Zoller, Cavity-assisted squeezing of a mechanical oscillator, Phys. Rev. A **79**, 063819 (2009).

[39] G. S. Agarwal and S. Huang, Strong mechanical squeezing and its detection, Phys. Rev. A **93**, 043844 (2016).

[40] J. Huang, D.-G. Lai, and J.-Q. Liao, Controllable generation of mechanical quadrature squeezing via dark-mode engineering in cavity optomechanics, Phys. Rev. A **108**, 013516 (2023).

[41] M. Asjad, G. S. Agarwal, M. S. Kim, P. Tombesi, G. Di Giuseppe, and D. Vitali, Robust stationary mechanical squeezing in a kicked quadratic optomechanical system, Phys. Rev. A **89**, 023849 (2014).

[42] X.-Y. Lü, J.-Q. Liao, L. Tian, and F. Nori, Steady-state mechanical squeezing in an optomechanical system via Duffing nonlinearity, Phys. Rev. A **91**, 013834 (2015).

[43] A. Kronwald, F. Marquardt, and A. A. Clerk, Arbitrarily large steady-state bosonic squeezing via dissipation, Phys. Rev. A **88**, 063833 (2013).

[44] B. Xiong, X. Li, S. L. Chao, and L. Zhou, Optomechanical quadrature squeezing in the non-Markovian regime, Opt. Lett. **43**, 6053 (2018).

[45] S. L. Braunstein and P. van Loock, Quantum information with continuous variables, Rev. Mod. Phys. **77**, 513 (2005).

[46] P. D. Drummond and Z. Ficek, *Quantum Squeezing* (Springer-Verlag, Berlin, 2004).

[47] C. M. Caves, K. S. Thorne, R. W. P. Drever, V. D. Sandberg, and M. Zimmermann, On the measurement of a weak classical force coupled to a quantum-mechanical oscillator. I. Issues of principle, Rev. Mod. Phys. **52**, 341 (1980).

[48] M. O. Scully and M. S. Zubairy, *Quantum Optics* (Cambridge University, Cambridge, England, 1997).

[49] M. R. Vanner, I. Pikovski, G. D. Cole, M. S. Kim, C. Brukner, K. Hammerer, G. J. Milburn, and M. Aspelmeyer, Pulsed quantum optomechanics, Proc. Natl. Acad. Sci. USA **108**, 16182 (2011).

[50] M. R. Vanner, J. Hofer, G. D. Cole, and M. Aspelmeyer, Cooling-by-measurement and mechanical state tomography via pulsed optomechanics, Nat. Commun. **4**, 2295 (2013).

[51] S. M. Meenehan, J. D. Cohen, G. S. MacCabe, F. Marsili, M. D. Shaw, and O. Painter, Pulsed excitation dynamics of an optomechanical crystal resonator near its quantum ground state of motion, Phys. Rev. X **5**, 041002 (2015).

[52] S. G. Hofer and K. Hammerer, Quantum control of optomechanical systems, Adv. At. Mol. Opt. Phys. **66**, 263 (2017).

[53] Y. Wang, J.-L. Wu, Y.-K. Feng, J.-X. Han, Y. Xia, Y.-Y. Jiang, and J. Song, Optimal control for robust photon state transfer in optomechanical systems, Ann. Phys. (Leipzig) **533**, 2000608 (2021).

[54] X. Wang, S. Vinjanampathy, F. W. Strauch, and K. Jacobs, Ultraefficient cooling of resonators: Beating sideband cooling with quantum control, Phys. Rev. Lett. **107**, 177204 (2011).

[55] F. Tebbenjohanns, M. L. Mattana, M. Rossi, M. Frimmer, and L. Novotny, Quantum control of a nanoparticle optically levitated in cryogenic free space, Nature (London) **595**, 378 (2021).

[56] Y.-H. Liu, X.-L. Yin, J.-F. Huang, and J.-Q. Liao, Accelerated ground-state cooling of an optomechanical resonator via shortcuts to adiabaticity, Phys. Rev. A **105**, 023504 (2022).

[57] D. Stefanatos, Maximising optomechanical entanglement with optimal control, Quantum Sci. Technol. **2**, 014003 (2017).

[58] J. Clarke, P. Sahium, K. Khosla, I. Pikovski, M. Kim, and M. Vanner, Generating mechanical and optomechanical entanglement via pulsed interaction and measurement, New J. Phys. **22**, 063001 (2020).

[59] D. Basilewitsch, C. P. Koch, and D. M. Reich, Quantum optimal control for mixed state squeezing in cavity optomechanics, Adv. Quantum Technol. **2**, 1800110 (2019).

[60] B. Xiong, L. Xun, S.-L. Chao, Z. Yang, W.-Z. Zhang, W. Zhang, and L. Zhou, Strong mechanical squeezing in an optomechanical system based on Lyapunov control, Photonics Res. **8**, 151 (2020).

[61] D. Dong and I. R. Petersen, *Learning and Robust Control in Quantum Technology* (Springer, New York, 2023).

[62] G. S. Agarwal, *Quantum Optics* (Cambridge University, Cambridge, England, 2013).

[63] W. Vogel and D. Welsch, *Quantum Optics* (Wiley, New York, 2006).

[64] We checked the correctness of the pulsed fields by back-substituting the pulsed field data obtained after the last iteration into the system evolution. We verified the results by either solving the covariance matrix $\mathbf{V}$ or solving the quantum master equation (4) under the replacement of $H_{\rm dis}(t) \to H_{\rm lin}(t)$. We find that the dynamic evolution of the squeezing degree $\mathcal{S}_b$ is consistent with the results obtained in this paper.

[65] J. F. Triana, A. F. Estrada, and L. A. Pachón, Ultrafast optimal sideband cooling under non-Markovian evolution, Phys. Rev. Lett. **116**, 183602 (2016).

[66] Y.-H. Liu, Y. Zeng, Q.-S. Tan, D. Dong, F. Nori, and J.-Q. Liao, Optimal control of linear Gaussian quantum systems via quantum learning control, Phys. Rev. A **109**, 063508 (2024).

[67] Y. S. Park and H. Wang, Resolved-sideband and cryogenic cooling of an optomechanical resonator, Nat. Phys. **5**, 489 (2009).

[68] A. Schliesser, O. Arcizet, R. Rivière, G. Anetsberger, and T. J. Kippenberg, Resolved-sideband cooling and position measurement of a micromechanical oscillator close to the Heisenberg uncertainty limit, Nat. Phys. **5**, 509 (2009).

[69] E. Verhagen, S. Deléglise, S. Weis, A. Schliesser, and T. J. Kippenberg, Quantum-coherent coupling of a mechanical oscillator to an optical cavity mode, Nature (London) **482**, 63 (2012).

[70] J. B. Hertzberg, T. Rocheleau, T. Ndukum, M. Savva, A. A. Clerk, and K. C. Schwab, Back-action-evading measurements of nanomechanical motion, Nat. Phys. **6**, 213 (2010).

[71] F. Massel, T. T. Heikkilä, J.-M. Pirkkalainen, S. U. Cho, H. Saloniemi, P. J. Hakonen, and M. A. Sillanpää, Microwave amplification with nanomechanical resonators, Nature (London) **480**, 351 (2011).

[72] F. Massel, S. U. Cho, J.-M. Pirkkalainen, P. J. Hakonen, T. T. Heikkilä, and M. A. Sillanpää, Multimode circuit optomechanics near the quantum limit, Nat. Commun. **3**, 987 (2012).

[73] M. Eichenfield, R. Camacho, J. Chan, K. J. Vahala, and O. Painter, A picogram- and nanometre-scale photonic-crystal optomechanical cavity, Nature (London) **459**, 550 (2009).

[74] M. Eichenfield, J. Chan, R. M. Camacho, K. J. Vahala, and O. Painter, Optomechanical crystals, Nature (London) **462**, 78 (2009).

[75] S. Gröblacher, K. Hammerer, M. R. Vanner, and M. Aspelmeyer, Observation of strong coupling between a micromechanical resonator and an optical cavity field, Nature (London) **460**, 724 (2009).

[76] W. Greiner and J. Reinhardt, *Field Quantization* (Springer-Verlag, Berlin, 1996).